Spectrochimica Acta Part A: Molecular and Biomolecular Spectroscopy 330 (2025) 125763

Contents lists available at ScienceDirect

Spectrochimica Acta Part A: Molecular and Biomolecular Spectroscopy

journal homepage: www.journals.elsevier.com/spectrochimica-acta-part-a-molecular-and-biomolecular-spectroscopy

Modulating room-temperature phosphorescence of D-π-A luminogens via methyl substitution, positional isomerism, and host–guest doping

Yang Zhu [a,1], Meiling Pan [b,1], Weirao Ji [a], Lei Ma [b,*], Yongtao Wang [a,*], Le Ruan [a]

[a] Guangxi Key Laboratory of Electrochemical and Magneto-chemical Function Materia, College of Chemistry and Bioengineering, Guilin University of Technology, Guilin 541004, China
[b] Tianjin International Center for Nanoparticles and Nanosystem, Tianjin University, Tianjin 300072, China

HIGHLIGHTS

- RTP of organic luminogens were finely tuned.
- 1 % 2M-TBTDA@PMMA film showed efficient RTP.
- Dynamic anti-counterfeiting and digital encryption were successfully constructed.
- Long reddish-brown or orange afterglows were achieved.
- FRET efficiency of the ternary doping systems were up to 90 %.

GRAPHICAL ABSTRACT

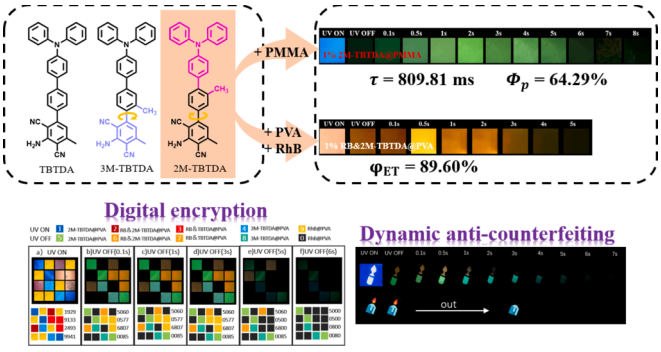

ARTICLE INFO

Keywords:
Room temperature phosphorescence
Host-guest doping
Long-lived phosphorescence
Long afterglow
Encryption

ABSTRACT

Organic room-temperature phosphorescence (RTP) luminogens have showed significant potential in the fields of diagnostics, sensing, and information encryption. However, it is difficult to achieve high RTP yield (Φ_P) and long RTP lifetime simultaneously. By methyl substitution, positional isomerism, and host–guest doping, three new D-π-A type luminogens named as TBTDA, 2M-TBTDA, and 3M-TBTDA were designed and synthesized, whose RTP properties were tuned and optimized. In various solvents and glassy THF solution, similar solvatochromism and phosphorescence nature of three luminogens were revealed. In poly (methyl methacrylate) (PMMA) and polyvinyl alcohol (PVA) matrixes, the luminogens showed high-contrast RTP properties. TBTDA emitted invisible afterglow in PMMA films, but with strong RTP and long green afterglow in PVA films. More importantly, 2M-TBTDA showed RTP and afterglow lifetimes of 809.81 ms and 8 s, as well as Φ_P of up to 0.64 in PMMA at 1 % doping concentration. Taking advantage of Foerster resonant energy transfer (FRET), reddish-brown or orange afterglow were observed, with emission maxima of 593–617 nm, RTP and afterglow lifetimes of 299–566 ms and 5–6 s, Φ_P of 0.34–0.46, as well as FRET efficiency of 70–90 %. Finally, dynamic anti-counterfeiting and digital encryption were successfully constructed via different fluorescence, RTP colors, and afterglow lifetimes. This work not only obtained an efficient host–guest doping RTP system, but also can be expected to provide more

* Corresponding authors.
E-mail addresses: lei.ma@tju.edu.cn (L. Ma), wyt_shzu@163.com (Y. Wang).
[1] Contributed equally.

https://doi.org/10.1016/j.saa.2025.125763
Received 4 December 2024; Received in revised form 9 January 2025; Accepted 15 January 2025
Available online 19 January 2025

theoretical guidance and experimental supports for molecular design, dynamic anti-counterfeiting and digital encryption.

1. Introduction

Organic room temperature phosphorescence (ORTP) materials can emit long afterglow, lasting for seconds, or even hours, after removing the radiation source. With large Stokes shift, excellent biocompatibility [1,2], long phosphorescence and afterglow lifetimes [14] and high triplet excitons utilization [15] ORTP materials have become a hot research topic and showed huge potential in the fields of diagnostics [3,4], organic light-emitting diodes (OLEDs) [12,13], sensing [5–7], and information encryption [2,8–11]. However, molecular design of ORTP materials with high Φ_P and ultralong RTP lifetime faces significant challenges due to spin-forbidden intersystem crossing between singlet and excited triplet states, and rapid energy dissipation induced by environmental oxygen and molecular motions [16,17]. By introducing heteroatoms such as carbonyl [18,19], sulfone [20], heavy atoms [21], oxygen [22], or nitrogen in molecular skeleton [23], spin-orbital coupling (SOC) [24] and intersystem crossing (ISC) [25–28] of ORTP materials are effectively improved, generating more triplet excitons. Thereby, Φ_P of ORTP materials are significantly enhanced, but generally accompanied by a decrease in RTP lifetime [29]. Delightingly, crystal engineering and host–guest doping can offer more rigid and anaerobic microenvironments to minimize oxygen quenching and molecular motions [30–36], resulting in simultaneous improvement of Φ_P and RTP lifetime. Compared with crystal engineering, host–guest doping can overcome the brittleness of crystals and the uncertainty of phosphorescence performance caused by crystallization conditions, and contribute to achieving flexible large-area display, low cost, outstanding processability, and various mechanical properties [30–33]. Of note, polymer matrixes, as the host materials, not only provide a rigid environment, but also affect the excited state energy levels, molecular conformations, and ISC of luminogens by intermolecular interactions between host and guest molecules [37–39]. As a result, manipulating internal mechanism of RTP and optimizing RTP performance of host–guest doping systems remains a challenging task [39,40].

Altering substituent groups and substitution positions are usually employed to achieve desired luminescent properties and explore structure–property relationship. For examples, Li et al. [40,41] adjusted RTP properties of phenothiazine derivatives by modifying push–pull electron ability of different substituent groups, and thereby found intermolecular π–π stacking interactions could be strengthened by electron-withdrawing substituent, leading to long-lived RTP. By 2-benzylmalononitrile (TCN), 3-amino-[1,1′-biphenyl]-2,4-dicarbonitrile (BTDA), and their halogenated derivatives [42,43], our research group obtained a series of dual-band emission host–guest doping systems with long-lived thermally activated delayed fluorescence (TADF) and RTP, and then found halogen atom substitution reduced intensity ratio between TADF and RTP due to the increased ISC transitions and phosphorescence radiation. Subsequently, six aryl acetonitrile (CBM) and aryl dicyanoaniline (AMBT) derivatives were synthesized and used as host and guest materials respectively based on ortho-, meta-, and *para*-position isomerization effect, where excellent TADF and RTP emission for m-CBM/o-AMBT were attributed to H-aggregation of m-CBM and the enhanced ISC for m-CBM and o-AMBT [42,43]. An et al. [44,45] modulated RTP of phenothiazine dioxide by different flexible alkyl chains and halogen atoms, highlighting a special C-Cl···π interaction for the development of ultralong phosphorescent materials. Although Φ_P and RTP lifetime of ORTP materials have been significantly optimized based on isomeric engineering and different substituent groups, a precise RTP performance prediction for luminogens with similar molecular structures is within sight but beyond reach, especially the doping systems with polymer matrixes as host materials [51–53].

As an efficient molecular design strategy for RTP luminogens, constructing electron donor (D)-electron acceptors (A) or D-π-A type molecular skeleton can effectively induce intramolecular charge transfer (ICT) mechanism and reduce the singlet–triplet energy gap (ΔE_{ST}) [46,47], and thereby boost the SOC between singlet charge transfer (^{1}CT) and triplet charge transfer (^{3}CT), generating more triplet excitons. Moreover, finely tuning the ΔE_{ST} of luminogens is still an important means of achieving dual state emission with RTP and TADF characteristics. Furthermore, triphenylamine (TPA) with propeller-shaped spatial molecular conformation is usually used as D, while dicyanoaniline (DCA) unit is a typical A due to the strong electron-withdrawing effect for CN [48,49]. Here, a D-π-A type luminogen named as TBTDA was firstly designed by choosing TPA and DCA as D and A units respectively, linked by a benzene bridge, whose molecular conformation and ΔE_{ST} were tuned by a methyl and different substitution sites, generating the corresponding luminogens called as 2M-TBTDA and 3M-TBTDA (Scheme S1). The experiments found that three luminogens showed significant solvatochromism in different solvents. Among them, 3M-TBTDA exhibited bigger ICT effect, followed by 2M-TBTDA and TBTDA. They presented phosphorescent nature in glassy THF solution, but unlike expected, TBTDA (0.22 eV) had a smaller ΔE_{ST} compared with 2M-TBTDA (0.36 eV) and 3M-TBTDA (0.25 eV). In the rigid PMMA environment, no visible afterglow was observed for TBTDA, but RTP and afterglow lifetimes, as well as Φ_P of 2M-TBTDA and 3M-TBTDA were up to 809.81 ms, 8 s, 0.64, 360.45 ms, 6 s, and 0.45 in sequence. Different from PMMA matrix, TBTDA showed time dependent dynamic afterglow, with RTP lifetimes of 496.94 ms and afterglow of 6 s, as well as Φ_P of 0.36 in PVA film, while the main photophysical parameters of 2M-TBTDA and 3M-TBTDA declined comprehensively, presenting RTP and afterglow lifetimes of 631.25 ms, 7 s, 326.93 ms, and 5 s, as well as Φ_P of 0.32 and 0.33 respectively. Ternary doping systems were constructed by PVA, TBTDA/2M-TBTDA/3M-TBTDA, and Rhodamine B (RB), with RTP lifetimes of 362.51–475.09 ms and reddish-brown or orange afterglow, lasting for 4–5 s. Of note, Φ_P and FRET efficiency of the ternary doping systems were up to 0.46 and 90 % in turn. Based on different afterglow lifetimes and colors, complex dynamic digital encryptions were successfully constructed. More importantly, the high contrast RTP properties exhibited by the three luminogens were discussed in detail through experimental analysis and theoretical calculations.

2. Results and discussion

Referring to previous reports, TBTDA, 2M-TBTDA, and 3M-TBTDA were prepared by using benzaldehyde derivatives and self-made 4-bromo-triphenylamine as raw materials, whose molecular structures and purities were characterized by ^{1}H NMR, ^{13}C NMR, HRMS, and high-performance liquid chromatography (HPLC) (Figs. S10–S21). TBTDA, 2M-TBTDA, and 3M-TBTDA showed similar absorption spectra and solvatochromism in various solvents, with two absorption bands centered at about 305 nm and 360 nm respectively, corresponding to π–π* and ICT transitions. Owing to bigger dipole moments for excited states than ground states, three luminogens presented significant solvatochromism and wavelength redshifts in emission spectra compared to UV–vis absorption spectra with the increasing solvent polarity, accompanied by stokes shifts of 157 nm, 163 nm, and 180 nm in sequence, as well as obvious color variance from deep blue, light blue, green to red (Fig. 1a–f). Lippert-Mataga plot indicated that 3M-TBTDA had largest ICT effect, followed by 2M-TBTDA and TBTDA, which should be attributed to the introduction of methyl groups increasing molecular distortion (Fig. S2). The relative fluorescence quantum yields (Φ_{PLQYs}) were tested and calculated by using quinine sulfate as a

reference (Table S1). Overall, the luminogens showed bright emission in diluted Tol, THF, and DMSO, especially in Tol and DMSO. Possibly because of the local state emission, the luminogens gave lower Φ_{PLQYs} in n-hexane compared to other solvents. More importantly, the luminogens emitted brilliant green afterglow in glassy THF solutions (77 K), indicating phosphorescence nature (Fig. 1g). However, visible afterglow could not be perceived for solid state samples of three luminogens due to molecular motions and oxygen quenching. Of note, three luminogens exhibited two phosphorescent peaks, located at 500 nm and 543 nm for TBTDA, 504 nm and 540 nm for 2M-TBTDA, 507 nm and 580 nm for 3M-TBTDA (Fig. 1h). Furthermore, two phosphorescent peaks of each luminogen had almost completely overlapping excitation spectra, which illustrated that the high-energy level phosphorescent peaks at 500 nm, 504 nm, and 507 nm should come from the lowest triplet state energy level (T_1) of unimolecular TBTDA, 2M-TBTDA, and 3M-TBTDA, while the low-energy level phosphorescent peaks were attributed to molecular fine vibration. Based on the fluorescence and phosphorescence emission maxima (77 K), ΔE_{ST} of TBTDA, 2M-TBTDA, and 3M-TBTDA were 0.22 eV, 0.36 eV, and 0.25 eV respectively (Table S1). Obviously, the introduction of methyl did not cause a decrease in ΔE_{ST}. As a control, c-TBTDA with the same molecular structure with TBTDA was prepared by using benzaldehyde derivatives and commercial 4-(diphenylamino) phenyl)boronic acid via a two-step synthesis reaction. According to the reported literature [50], commercial triphenylamine (TPA) contained trace DPN-1 and DPN-2, which might lead to the presence of trace TBTDA-1 and TBTDA-2 due to similar chemical property between TPA and DPN-1/DPN-2 (Scheme S2). However, no impurity peak was observed in HPLC (Fig. S13), and molecular ion peak of DPN-1/DPN-2 was not captured either in HRMS spectrum (Fig. S12). By contrast, c-TBTDA and TBTDA exhibited negligible differences in fluorescence, phosphorescence spectra, and afterglow, demonstrating the minor impact of commercial triphenylamine's trace impurities on luminescence performance in glassy THF solutions.

By physical encapsulation, doping, covalent bonding, and cross-linking, phosphors were introduced into polymer matrices to suppress molecular motions and oxygen diffusion. Among of them, PVA and PMMA were the most common polymer matrices, while the solution-doping was a simple and efficient method. A series of doping films were prepared and optimized by dissolving phosphors and PVA/PMMA, as well as tuning their mass ratios from 0.5 %, 1 %, 5 % to 10 %. Taking 1 % TBTDA@PVA film as an example, it was prepared by dissolving TBTDA and PVA in THF-H_2O solution at the mass doping ratios of 1:100, and the other doping films were named according to this rule. Surprisingly, TBTDA@PMMA films at different doping concentrations emitted invisible afterglow after 60–180 s irradiation with a 365 nm ultraviolet lamp (Fig. S3), but with bright green or yellow-green afterglow for 2M-TBTADA@PMMA and 3M-TBTDA@PMMA films at different doping concentrations (Figs. S5a and S6a). When the TBTDA@PMMA films were cooled to 77 K, or placed to in a nitrogen atmosphere, they presented green afterglow lasting for over 3 s (Fig. S3). Therefore, we speculated that PMMA had inferior inhibition ability on molecular motions and oxygen diffusion due to weak intermolecular hydrogen bonds, resulting in invisible afterglow for the TBTDA@PMMA films, while bright afterglows of 2M-TBTDA@PMMA and 3M-TBTDA@PMMA films should lie in the improved phosphorescent radiation rate (K_P). Notably, 1 % 2M-TBTDA@PMMA and 5 % 3M-TBTDA@PMMA films

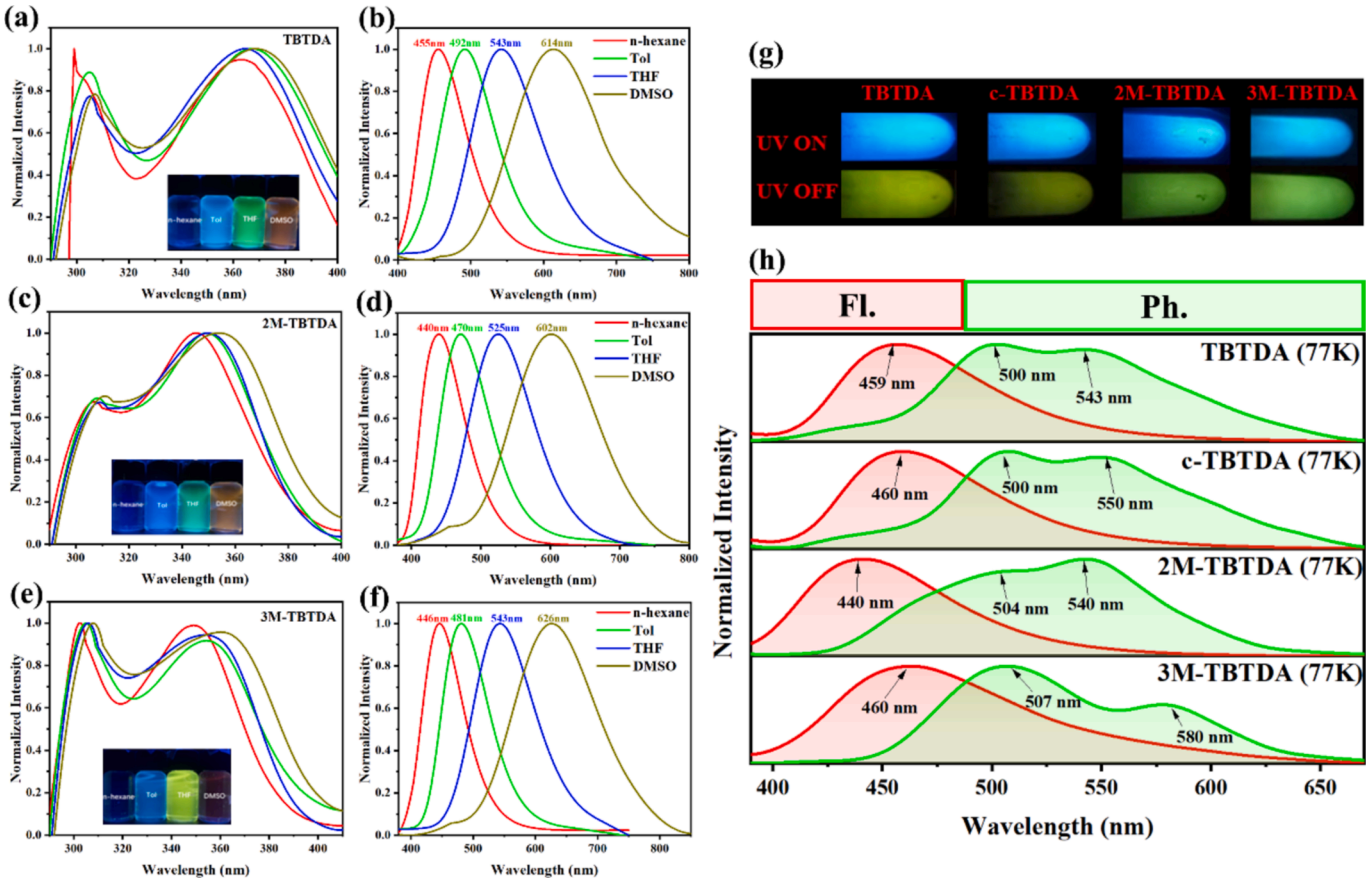

Fig. 1. (a) (c) (e)Normalized UV–vis absorption and (b) (d) (f) fluorescence emission spectra of TBTDA, 2M-TBTDA, and 3M-TBTDA in different solvents (λ_{ex}: 365 nm, solution concentration: 10^{-5} M); (g) Photos of TBTDA, c-TBTDA, 2M-TBTDA and 3M-TBTDA by turning on/off a 365 nm UV light lamp at 77 K in THF solution; (h) Fluorescence and phosphorescence emission spectra of TBTDA, c-TBTDA, 2M-TBTDA and 3M-TBTDA at 77 K in THF solution (λ_{ex}: 365 nm, solution concentration: 10^{-5} M).

showed the strongest RTP emission intensity and longest afterglow lifetimes in different doping concentrations, with RTP and afterglow lifetimes of 809.81 ms, 8 s, 360.45 ms, and 6 s, as well as Φ_P of 0.64 and 0.45 in sequence, whose fluorescence and RTP emission maxima were located at 477 nm, 481 nm, 477 nm and 500 nm in turn (Figs. S5 and S6). Compared with fluorescence and RTP emission maxima in THF solution at 77 K, fluorescence emission maxima of 1 % 2M-TBTDA@PMMA and 5 % 3M-TBTDA presented red shifts of 37 nm and 17 nm respectively, while their RTP emission maxima showed blue shifts of 23 nm and 7 nm in sequence, leading to the decreasing ΔE_{ST} for 2M-TBTDA (0.02 eV) and 3M-TBTDA (0.12 eV) in PMMA films, which might be due to the enhanced intermolecular interactions in host and guest materials. Considering the close fluorescence and phosphorescence emissions, the varied temperature phosphorescence spectra of 1 % 2M-TBTDA@PMMA and 5 % 3M-TBTDA@PMMA films were investigated, which indicated phosphorescence intensity of 1 % 2M-TBTDA@PMMA and 5 % 3M-TBTDA@PMMA films presented continued to decrease from 77 K, 127 K, 187 K, 237 K to 297 K (Figs. S5b and S6b). Thereby, long afterglow of two doping films should come from RTP rather than thermal activated delayed fluorescence (TADF). RTP materials with long lifetime and high Φ_P are of interest but challenging. Recently, Deng et al. [24] designed and synthesized a phosphor based on heteroaromatic sulfone-locked triphenylamine core, whose RTP lifetime and Φ_P were up to 818 ms and 0.20 respectively in PMMA matrix. Phenanthrene (Phe) was doped with the monmers (methyl methacrylate, MMA) followed by in situ polymerization to obtain well-dispersed Phe@PMMA systems, presenting RTP and afterglow lifetimes of 1.27 s and 12 s in turn [54]. When 7H-benzo[c]carbazole (BCz) and its derivatives were doped into PMMA, RTP lifetime of 1.3 s was achieved [55]. By the chemical locking of internal rotation units in advance, Zhang et al. [56] obtained two new luminogens, which emitted green and blue ultralong RTP in PMMA film, with lifetimes of 2146 ms and 2656 ms, respectively. By doping of synthesized polymeric phosphors into PMMA matrix, long-lived RTP systems (1258.62 ms) were obtained, even in an aqueous environment [57]. By contrast, such a high Φ_P (0.64) combined with long RTP (809.81 ms) and afterglow (8 s) lifetimes for 1 % 2M-TBTDA@PMMA was rare in existing reports.

Owing to stronger intermolecular hydrogen bonding for PVA film than PMMA film, molecular vibration and oxygen diffusion might be better suppressed, leading to long-lived RTP. Among of them, 1 % TBTDA@PVA film showed RTP lifetimes of 496.94 ms and afterglow of 6 s, as well as Φ_P of 0.36, which confirmed the stronger inhibitory effects on molecular motions and oxygen diffusion for PVA than PMMA matrix. Noteworthy, the corresponding photophysical parameters of 1 % 2M-TBTDA@PVA and 0.5 % 3M-TBTDA@PVA films were 631.25 ms, 7 s, 0.32 and 326.93 ms, 5 s, 0.33 in turn (Figs. S7–S8 and Table S4). Further comparison showed that Φ_P of 1 % 2M-TBTDA@PMMA (0.64) and 5 % 3M-TBTDA@PMMA (0.45) films were 1.94 and 1.41 times those of 1 % 2M-TBTDA@PVA (0.32) and 0.5 % 3M-TBTDA@PVA (0.33) films in sequence, and with longer RTP and lifetimes for the first two than the latter two (Figs. 2–3 and Table S4), fully demonstrating the importance of polymer matrix selection and the corresponding unpredictable impact on RTP properties. In above-mentioned PVA films, 2M-TBTDA displayed the longest RTP and afterglow lifetimes, as well as equivalent Φ_P to TBTDA. Overall, 2M-TBTDA showed the best RTP performance not only in PVA but also in PMMA film (Figs. 2a–b and 3a–b). Of note, 1 % c-TBTDA@PVA and 1 % TBTDA@PVA films showed the same fluorescence and RTP spectra, as well as equally long afterglow lifetime, whose fluorescence (490 nm) and RTP maxima (550 nm) gave bathochromic-shifts of 31 nm and 50 nm in turn compared with those in the diluted THF solution at 77 K. As a speculation, fluorescence and RTP emission of 1 % c-TBTDA@PVA and 1 % TBTDA@PVA films should come from aggregates c-TBTDA and TBTDA. More interestingly, 1 % c-TBTDA@PVA and 1 % TBTDA@PVA films displayed an obvious

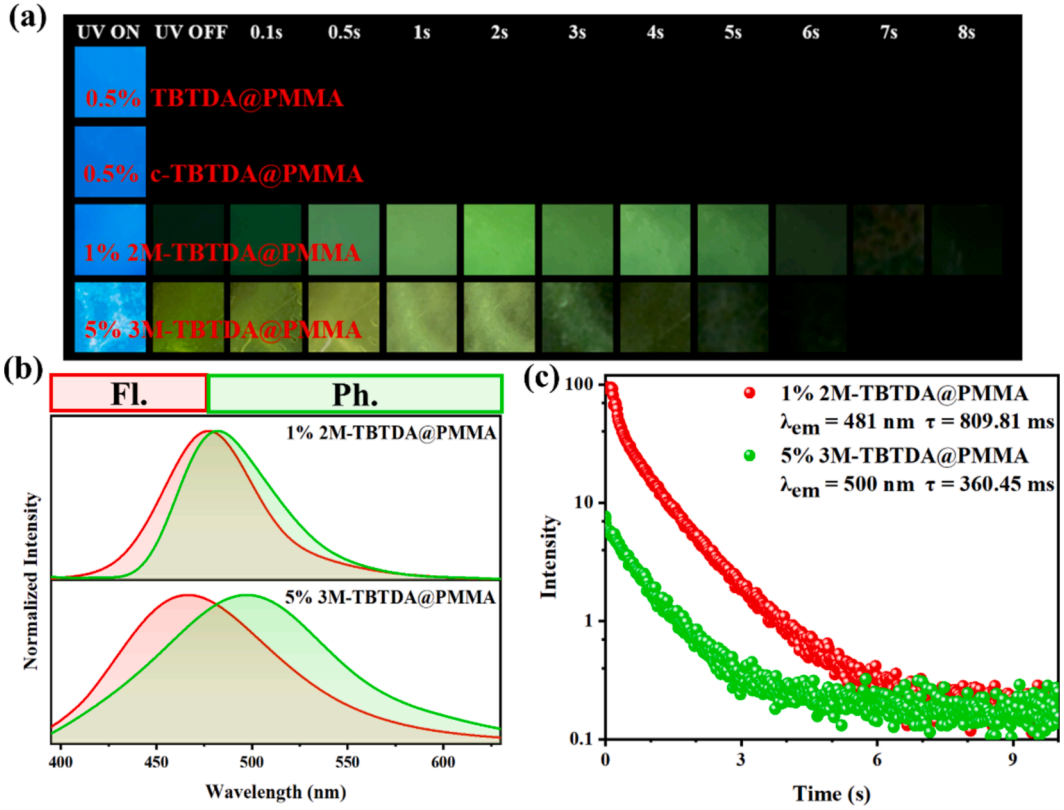

Fig. 2. (a) Photos of 0.5 % TBTDA@PMMA, 0.5 % c-TBTDA@PMMA, 1 % 2M-TBTDA@PMMA and 5 % 3M-TBTDA@PMMA films by turning on/off a 365 nm UV lamp; (b) Normalized fluorescence and phosphorescence emission spectra of 1 % 2M-TBTDA@PMMA and 5 % 3M-TBTDA@PMMA films (λ_{ex}: 365 nm); (c) The time-resolved phosphorescent decay curves of 1 % 2M-TBTDA@PMMA and 5 % 3M-TBTDA@PMMA films.

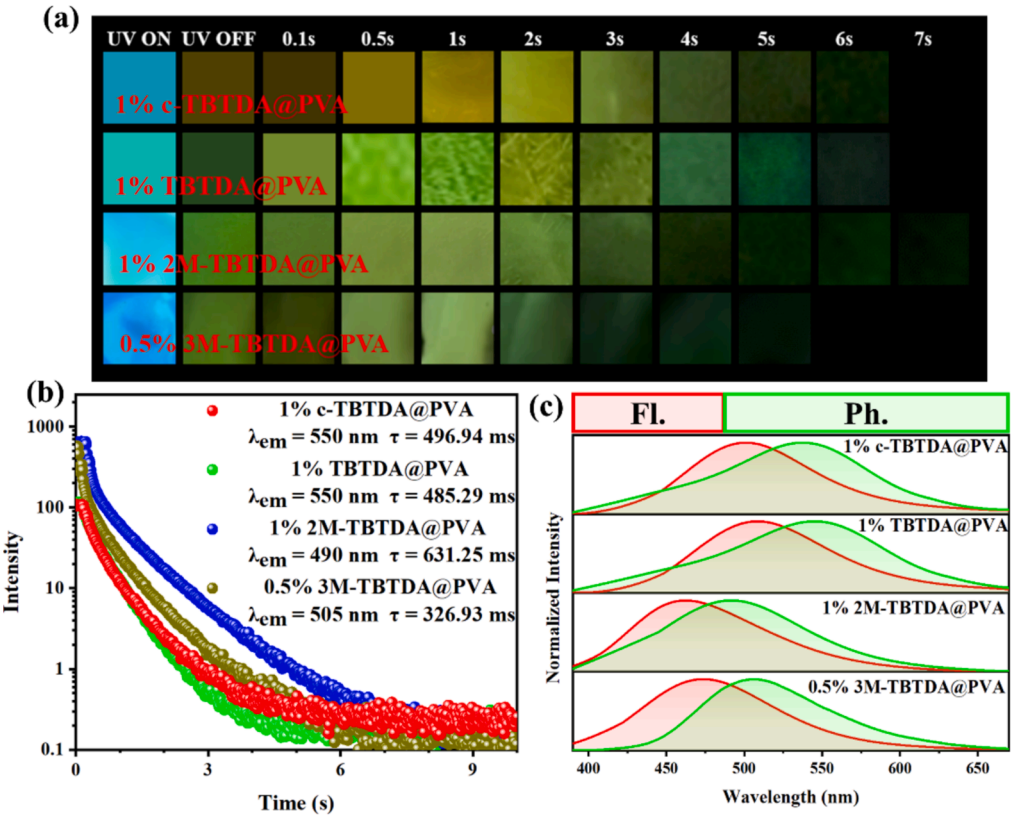

Fig. 3. (a) Photos of 1 % c-TBTDA@PVA, 1 % TBTDA@PVA, 1 % 2M-TBTDA@PVA and 0.5 % 3M-TBTDA@PVA films by turning on/off a 365 nm UV lamp; (b) The time-resolved phosphorescent decay curves of 1 % c-TBTDA@PVA, 1 % TBTDA@PVA, 1 % 2M-TBTDA@PVA and 0.5 % 3M-TBTDA@PVA films (τ_d = 0.1 ms); (c) Normalized fluorescence and phosphorescence emission spectra of 1 % c-TBTDA@PVA, 1 % TBTDA@PVA, 1 % 2M-TBTDA@PVA and 0.5 % 3M-TBTDA@PVA films at a 365 nm UV lamp.

dynamic afterglow, presenting a high-contrast color transition from orange yellow to green (Fig. 3), which should be due to multi-state emission with different lifetimes. To clarify the above mechanism, delayed spectra of 5 % TBTDA@PVA and 5 % c-TBTDA@PVA films were investigated under different delay times. When delay time (τ_d) was 1 ms, 5 % TBTDA@PVA film displayed a wide RTP emission spectrum, speculated to include delayed fluorescence, monomer and aggregate RTP. As τ_d continued to increase to 3 ms, the emission spectrum became narrower and remained stable (monomer RTP) until τ_d = 30 ms, and the corresponding tunable CIE chromaticity coordinates were shown in Fig. 4b. Similar to 5 % TBTDA@PVA film, 5 % c-TBTDA@PVA film also gave a wide RTP emission at τ_d = 1 ms. As τ_d continued to increase to 3 ms, the emission peak gave bathochromic shifts of 27 nm, accompanied by the narrowing of the emission spectrum and the appearance of a shoulder peak at 580 nm. With further increase in τ_d from 5 ms to 30 ms, only monomer RTP remained. Thereby, 5 % c-TBTDA@PVA film also presented tunable CIE chromaticity coordinates, whose multi-state emission characteristics were confirmed.

The geometry optimizations of TBTDA, 2M-TBTDA, and 3M-TBTDA were performed at the B3LYP/def2-TZVP level using D4 dispersion correction, and all single-point calculations were performed at B3LYP/def2-TZVP level. The results showed that the highest occupied molecular orbitals (HOMO) electron density distribution of three luminogens concentrated on TPA unit, while their lowest unoccupied molecular orbitals (LUMO) electron density mainly distributed on benzene bridge and dicyanoaniline unit, indicating typical ICT effect, which was responsible for solvatochromism of three luminogens (Fig. 5d). Compared with TBTDA, the introduction of methyl group leaded to the reduced LUMO energy levels for 2M-TBTDA and 3M-TBTDA, but HOMO energy levels showed increase of 0.01 eV and decrease of 0.04 eV in turn, and thereby producing increasing optical gaps. Overall, 2M-TBTDA and 3M-TBTDA showed blue shifted fluorescence emission in comparation to TBTDA in various solvents, which was consistent with the increasing optical gaps for 2M-TBTDA and 3M-TBTDA than TBTDA. Furthermore, S_1 state energy levels of TBTDA, 2M-TBTDA and 3M-TBTDA were 2.28, 2.43, and 2.38 eV, corresponding to blue-shifted fluorescence emission maxima for 2M-TBTDA than TBTDA and 3M-TBTDA very well in various solutions and PVA films. Three luminogens had three triplet states T_1, T_2, and T_3 near S_1 state, and TBTDA showed smaller energy gaps and bigger spin orbit coupling constants (ξ) between S_1 and T_1, T_2, T_3 compared with 2M-TBTDA and 3M-TBTDA, contributing to boosting the generation of more triplet excitons for TBTDA than 2M-TBTDA and 3M-TBTDA. However, $\xi(T_1 \rightarrow S_0)$ (0.153 cm^{-1}) of TBTDA were significantly lower than those of 2M-TBTDA (0.822 cm^{-1}) and 3M-TBTDA (0.735 cm^{-1}), which was not conducive to boost phosphorescence radiation and compete with RTP quenching caused by oxygen and molecular motions (Fig. 5a–c), thereby 1 % 2M-TBTDA@PMMA films and 1 % 3M-TBTDA@PMMA films could emit bright RTP, but not for 1 % TBTDA@PMMA film in the atmospheric environment. Of note, the experimental results showed that 2M-TBTDA gave the minimum ΔE_{ST} in PMMA (0.02 eV) and PVA (0.16 eV) films, which was inconsistent with theoretical calculations due to the neglected intermolecular interactions between host and guest materials. Theoretically, TBTDA should show longest afterglow and RTP lifetimes due to small energy gaps and big ξ between S_1 and T_1, T_2, T_3, as well as small $\xi(T_1 \rightarrow S_0)$.

Owing to deep penetration and weak destruction to biological tissues, as well as the enhanced non radiative decay, long wavelength afterglow materials have important application prospects in bioimaging and biosensing, but they are difficult to obtain. Recently, FRET theory and heavy-atom effect have played an important role in obtaining red and near-infrared materials. Based on FRET theory and RTP

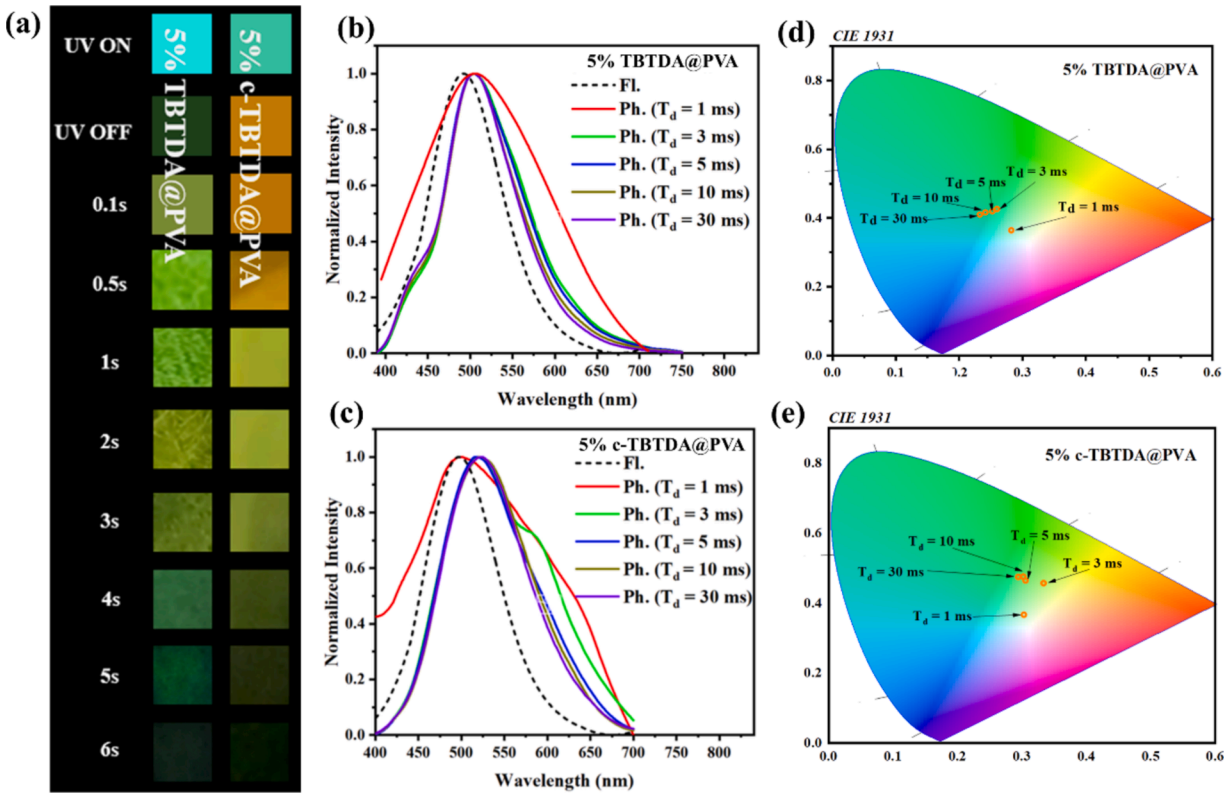

Fig. 4. (a) Photos of 5 % TBTDA@PVA and 5 % c-TBTDA@PVA films by turning on/off 365 nm UV light lamps; (b)–(c) Delayed RTP spectra of 5 % TBTDA@PVA and 5 % c-TBTDA@PVA @PVA films; (d)–(e) CIE chromaticity coordinates of 5 % TBTDA@PVA and 5 % c-TBTDA@PVA films.

performance of the above mentioned doping films, four ternary doping systems named as 1 % RB&TBTDA@PVA, 1 % RB&2M-TBTDA@PMMA, 1 % RB&2M-TBTDA@PVA, and 0.5 % RB&3M-TBTDA@PVA were constructed and investigated, corresponding to the mass ratio of 0.2:1:100 between RhB, TBTDA/2M-TBTDA, and PVA/PMMA, as well as 0.2:0.5:100 between RhB, 3M-TBTDA, and PVA. The ternary doping systems showed reddish-brown or orange afterglow, with emission maxima of 593–617 nm, indicating that effective energy transfer from three luminogens to RhB (Figs. 6 and S9). FRET efficiencies were calculated by decay lifetimes, listed in Table S3. By contrast, 1 % RB&2M-TBTDA@PMMA presented the shortest RTP (114.91 ms) and afterglow (2 s) lifetimes, the lowest FRET efficiency (14 %) (Table S3 and Fig. S9), which were attributed to the terrible overlap between RTP spectra of 2M-TBTDA and absorption spectra of Rhodamine B (RhB) in PMMA film, while 1 % RB&TBTDA@PVA, 1 % RB&2M-TBTDA@PVA and 0.5 % 3M-TBTDA@PVA had RTP lifetimes of 299–566 ms, afterglow lifetimes of 5–6 s, Φ_P of 0.34–0.46, as well as FRET efficiency of up to 70–90 % due to the excellent spectral overlap. It was worth mentioning that the ternary doping systems displayed postponed afterglow emission, showing the brightest afterglow after 0.5 s turning off a UV lamp, which should be due to the extension of energy transfer routine.

3. Application

Based on different afterglow lifetimes and colors, the dynamic process of candle extinguishing was simulated by choosing 1 % 2M-TBTDA@PMMA and 1 % RB&2M-TBTDA@PMMA as the “flame and candle”. Switching on a 365 UV lamp, bright white flame and candle were observed, which became brown flame and green candle after switching off the 365 UV lamp. The candle went out after 3 s, leaving only the green candle, which lasted for another 3 s (Fig. 7a). As shown in Fig. 7b, a series of doping films were selected, corresponding to ten numbers from 0 to 9 respectively via different fluorescence and afterglow colors. Taking the first line as an example, four pictures of different colors represented numbers “1929” under UV irradiation, which transformed into numbers “5060” and “5000” as time passed after turning off the UV lamp. Thereby, complex dynamic digital encryption was implemented by switching on/off a 365 nm UV lamp.

4. Conclusion

Three new D-π-A type luminogens were designed and synthesized, whose luminescent properties could be tuned by introducing a methyl group and altering its substitution positions, as well as choosing different host materials. Owing to the ICT effect, the luminogens showed silimar solvatochromism in different dilution solvents. In glassy THF solution, phosphorescence nature of three luminogens was revealed. The weak $\xi(T_1 \rightarrow S_0)$ for TBTDA, together with inferior inhibition ability on molecular motions and oxygen for PMMA matrix resulted in invisible afterglow for TBTDA@PMMA films at different doping concentrations. 1 % 2M-TBTDA@PMMA film showed RTP lifetimes of 809.81 ms, afterglow lifetimes of 8 s, and Φ_P of up to 0.64, demonstrating excellent RTP performance, which were attributed to the enhanced $\xi(T_1 \rightarrow S_0)$ and tiny ΔE_{ST} (0.02 eV). Comparison of different RTP properties of three luminogens in PMMA and PVA further confirmed the importance of polymer matrix selection and their unpredictable impact. TBTDA showed significantly enhanced in PVA films compared with in PMMA films, while 2M-TBTDA and 3M-TBTDA presented the opposite result. The former was due to the stronger inhibitory effects on molecular motions and oxygen diffusion for PVA than PMMA matrix, whereas the latter lay in different intermolecular interactions between host and guest materials and the resulting alterations in molecular energy levels and ISC. Based on FRET theory and the excellent spectral overlap, 1 % RB&TBTDA@PVA, 1 % RB&2M-TBTDA@PVA, and 0.5 % RB&3M-TBTDA@PVA achieved reddish-brown or orange long afterglow, with emission maxima of 593–617 nm, RTP lifetimes of 299–566 ms,

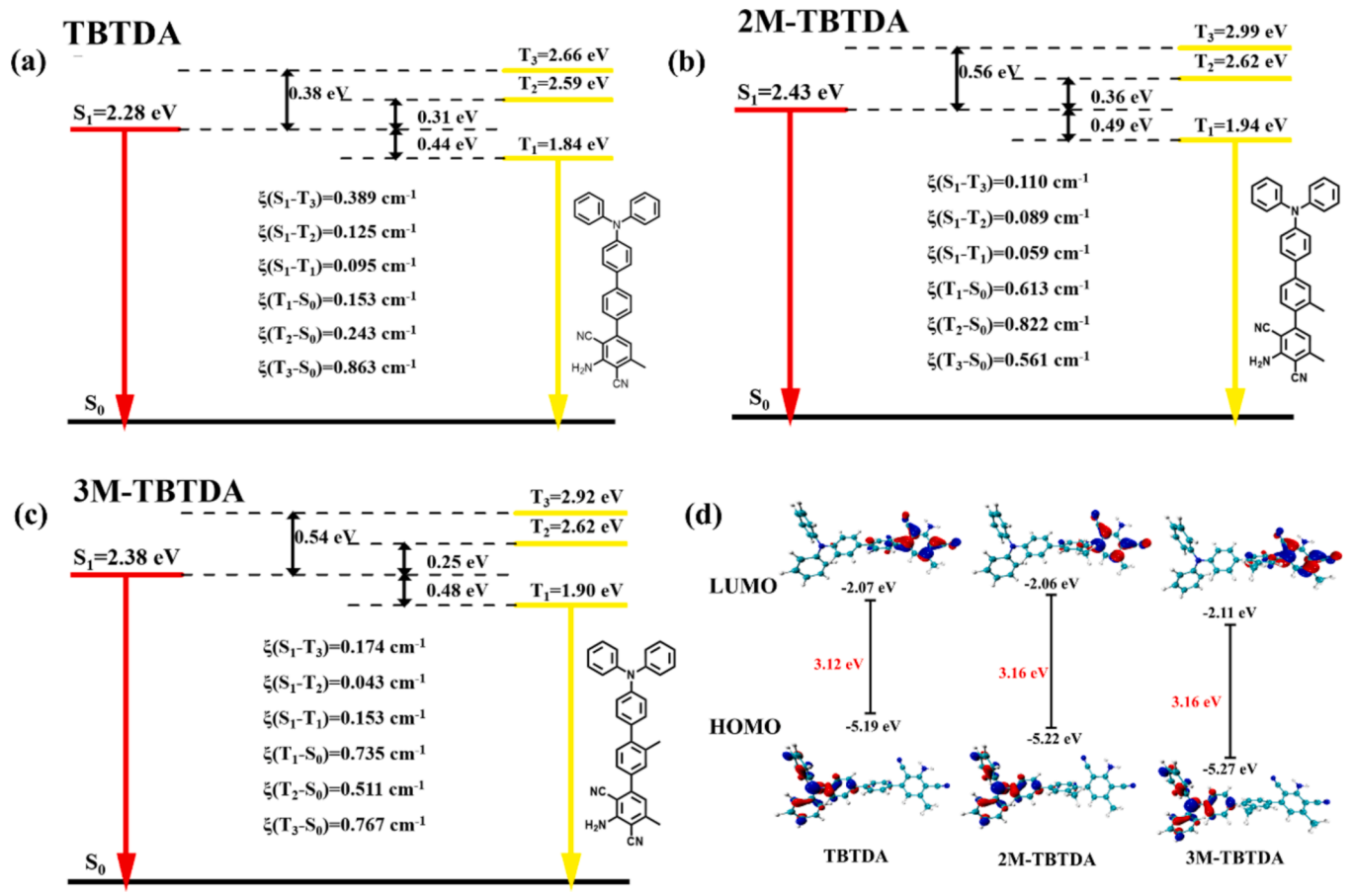

Fig. 5. Energy levels and spin orbit coupling constants (ξ) of (a) TBTDA, (b) 2M-TBTDA, (c) 3M-TBTDA; (d) HOMO and LUMO distribution of TBTDA, 2M-TBTDA, and 3M-TBTDA.

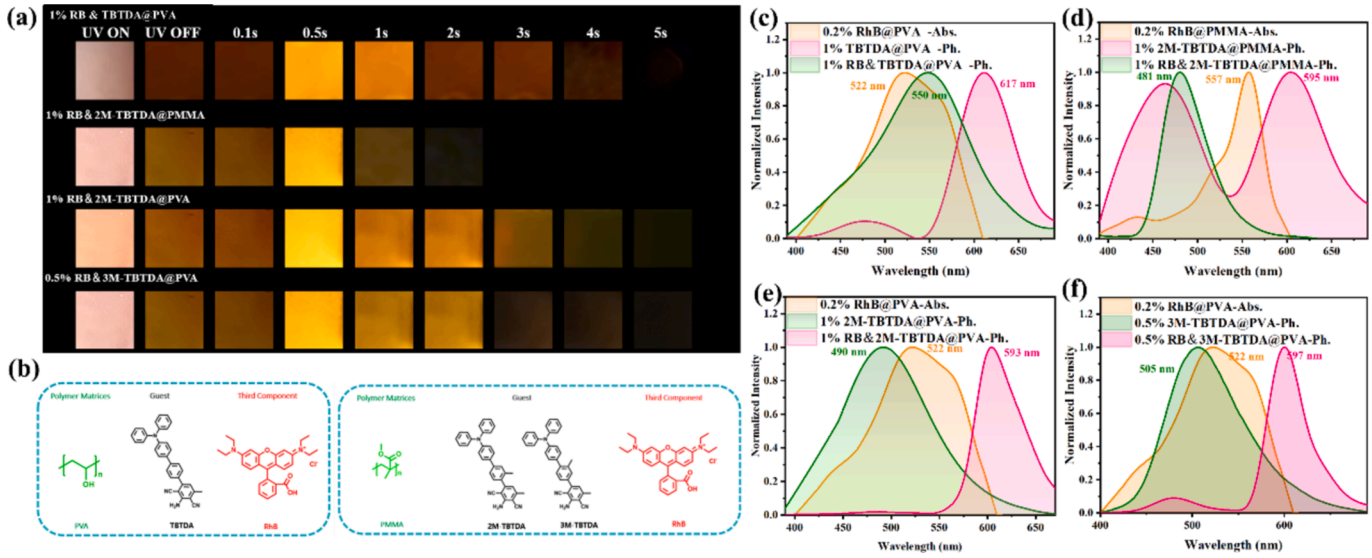

Fig. 6. (a) Photos of 1 % RB&TBTDA@PVA, 1 % RB&2M-TBTDA@PMMA, 1 % RB&2M-TBTDA@PVA and 0.5 % 3M-TBTDA @PVA by turning on/off 365 nm UV light lamps; (b) Chemical structures of polymer matrices and dopants; (c)–(f) Normalized UV–vis absorption and fluorescence and phosphorescence emission spectra of 1 % RB&TBTDA@PVA, 1 % RB&2M-TBTDA@PMMA, 1 % RB&2M-TBTDA@PVA and 0.5 % 3M-TBTDA@PVA.

afterglow lifetimes of 5–6 s, Φ_P of 0.34–0.46, as well as FRET efficiency of 70–90 %. Based on different afterglow lifetimes, Fluorescence and afterglow colors, the dynamic anti-counterfeiting and digital encryption were successfully constructed. This work not only obtained a new host–guest doping RTP system with long afterglow and high Φ_P, but also can be expected to provide more theoretical guidance and experimental supports for the construction of host guest doping system, dynamic anti-counterfeiting and digital encryption.

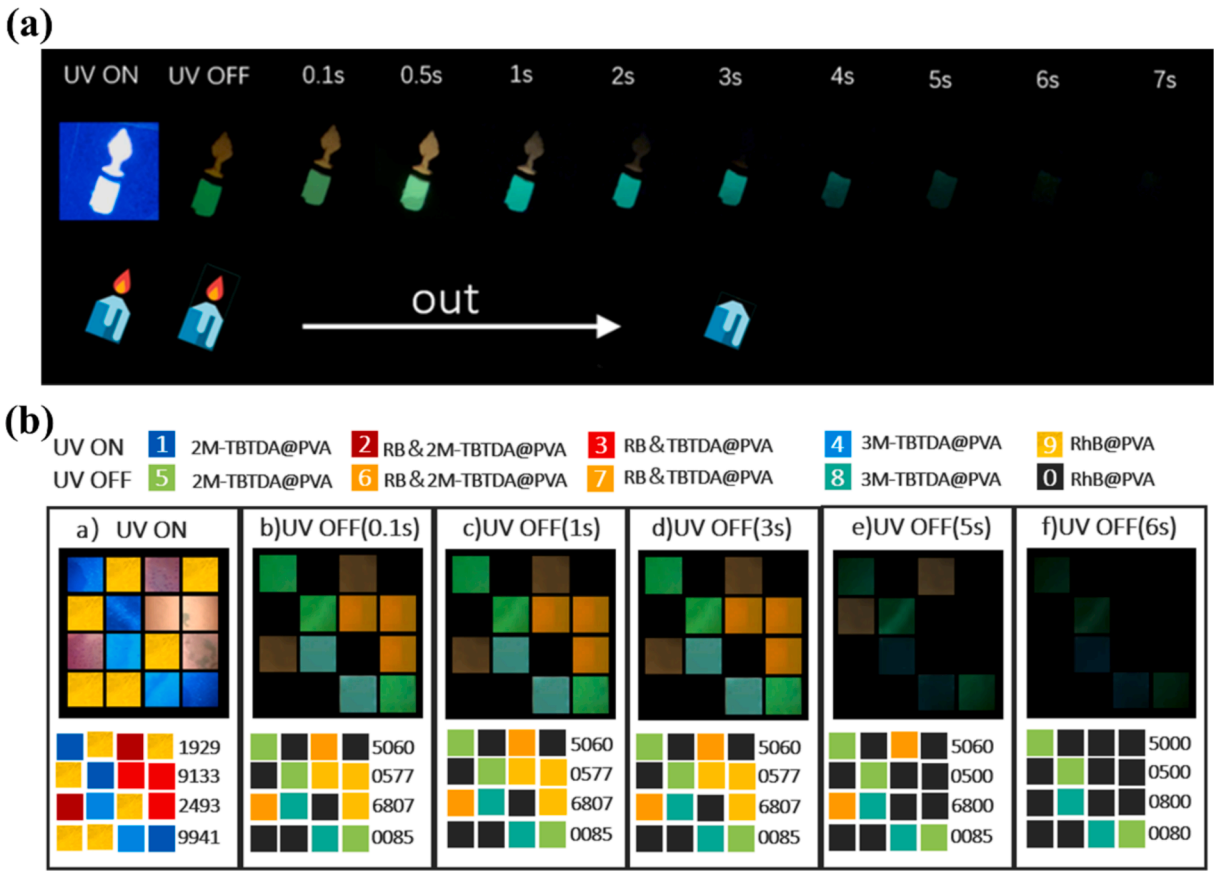

Fig. 7. (a) Graphic applications by using 1 % 2M-TBTDA@PMMA and 1 % RB&2M-TBTDA@PMMA; (b) Encryption applications by using 1 % 2M-TBTDA@PVA, 1 % RB&2M-TBTDA@PVA, 1 % RB&TBTDA @PVA and 0.5 % 3M-TBTDA@PVA doping systems.

Declaration of competing interest

The authors declare that they have no known competing financial interests or personal relationships that could have appeared to influence the work reported in this paper.

Acknowledgments

This work was supported by the Guangxi Natural Science Foundation (Grant No. 2024GXNSFAA999457 and 2020GXNSFAA159147), the National Natural Science Foundation of China (Grant No. 21766030).

Appendix A. Supplementary material

Supplementary data to this article can be found online at https://doi.org/10.1016/j.saa.2025.125763.

Data availability

The data that has been used is confidential.

References

[1] S.M.A. Fateminia, Z. Mao, S. Xu, Z. Yang, Z. Chi, B. Liu, Organic nanocrystals with bright red persistent room-temperature phosphorescence for biological applications, Angew. Chem. Int. Ed. 56 (2017) 12160–12164, https://doi.org/10.1002/anie.201705945.

[2] Y. Zhang, H. Li, M. Yang, W. Dai, J. Shi, B. Tong, Z. Cai, Z. Wang, Y. Dong, X. Yu, Organic room-temperature phosphorescence materials for bioimaging, Chem. Commun. 59 (2023) 5329–5342, https://doi.org/10.1039/d3cc00923h.

[3] X. Dai, Z. Liu, Y. Ge, P. Wei, Ultralong aqueous organic room-temperature phosphorescent probes for in vivo time-resolved bioimaging, TRAC-Trend Anal. Chem. 168 (2023) 117339, https://doi.org/10.1016/j.trac.2023.117339.

[4] Q. Ren, X. Dai, R. Cen, Y. Luo, M. Li, Z. Zhang, Q. Bai, Z. Tao, X. Xiao, A cucurbit[8]uril-based supramolecular phosphorescent assembly: cell imaging and sensing of amino acids in aqueous solution, Chin. Chem. Lett. 35 (2024) 110022, https://doi.org/10.1016/j.cclet.2024.110022.

[5] W. Huang, Y. Zhu, X. Xie, G. Tang, K. Zhou, L. Song, Z. He, Utilizing weakly donor-acceptor ternary pi-conjugated architecture to achieve single-component white luminescence and stimulus-responsive room-temperature phosphorescence, Chem. Sci. 15 (2024) 12316–12325, https://doi.org/10.1039/d4sc02525c.

[6] A. Lv, W. Gong, K. Lv, Q. Ma, Z. An, H. Ma, Molecular insight into the water-induced enhancement of room-temperature phosphorescence in organic aggregates, Adv. Opt. Mater. 12 (2023) 2301937, https://doi.org/10.1002/adom.202301937.

[7] D.X. Ma, Z.Q. Li, K. Tang, Z.L. Gong, J.Y. Shao, Y.W. Zhong, Nylons with highly-bright and ultralong organic room-temperature phosphorescence, Nat. Commun. 15 (2024) 4402, https://doi.org/10.1038/s41467-024-48836-7.

[8] X. Chen, W. Dai, X. Wu, H. Su, C. Chao, Y. Lei, J. Shi, B. Tong, Z. Cai, Y. Dong, Fluorene-based host-guest phosphorescence materials for information encryption, Chem. Eng. J. 426 (2021) 131607, https://doi.org/10.1016/j.cej.2021.131607.

[9] Z.Y. Chen, Z. Chen, Y.Q. Zhu, M.Z. Zhuo, G.Y. Yang, X.H. Wang, M.X. Wu, Ultralong blue organic room-temperature phosphorescence promoted by green assembly, Adv. Funct. Mater. 34 (2024) 2408023, https://doi.org/10.1002/adfm.202408023.

[10] J. Yang, X. Zhen, B. Wang, X. Gao, Z. Ren, J. Wang, Y. Xie, J. Li, Q. Peng, K. Pu, Z. Li, The influence of the molecular packing on the room temperature phosphorescence of purely organic luminogens, Nat. Commun. 9 (2018) 840, https://doi.org/10.1038/s41467-018-03236-6.

[11] S. Yi, S. Jiang, K. Wang, H. Wu, Y. Zhou, L. Qu, C. Yang, Electronic modulation induced luminescence from triphenylamine derivative and temperature sensor application, Adv. Opt. Mater. 12 (2023) 2301601, https://doi.org/10.1002/adom.202301601.

[12] X. Yan, H. Peng, Y. Xiang, J. Wang, L. Yu, Y. Tao, H. Li, W. Huang, R. Chen, Recent advances on host-guest material systems toward organic room temperature phosphorescence, Small 18 (2022) 2104073, https://doi.org/10.1002/smll.202104073.

[13] Y. Zhou, C. Ma, L. Zhang, J. Song, M. Sun, C. Li, Q. Sun, W. Yang, S. Xue, Multifunctional applications of organic light-emitting diodes and room temperature phosphorescence based on benzoyl-fluorene hybrid molecules, Dyes Pigm. 227 (2024) 112179, https://doi.org/10.1016/j.dyepig.2024.112179.

[14] Y. Zhang, X. Chen, J. Xu, Q. Zhang, L. Gao, Z. Wang, L. Qu, K. Wang, Y. Li, Z. Cai, Y. Zhao, C. Yang, Cross-linked polyphosphazene nanospheres boosting long-lived

organic room-temperature phosphorescence, J. Am. Chem. Soc. 144 (2022) 6107–6117, https://doi.org/10.1021/jacs.2c02076.
[15] J. Fan, Y. Zhang, K. Zhang, J. Liu, G. Jiang, F. Li, L. Lin, C.K. Wang, Theoretical arrangement of thermally activated delayed fluorescence as host for fluorescent emitter with blue to red emission, Spectrochim. Acta. A. Mol. Biomol Spectrosc. 219 (2019) 44–52, https://doi.org/10.1016/j.saa.2019.04.033.
[16] L. Ma, Y. Liu, H. Tian, X. Ma, Switching singlet exciton to triplet for efficient pure organic room-temperature phosphorescence by rational molecular design, JACS Au 3 (2023) 1835–1842, https://doi.org/10.1021/jacsau.3c00268.
[17] Y. Zhang, L. Gao, X. Zheng, Z. Wang, C. Yang, H. Tang, L. Qu, Y. Li, Y. Zhao, Ultraviolet irradiation-responsive dynamic ultralong organic phosphorescence in polymeric systems, Nat. Commun. 12 (2021) 2297, https://doi.org/10.1038/s41467-021-22609-y.
[18] Y. He, J. Wang, Q. Li, S. Qu, C. Zhou, C. Yin, H. Ma, H. Shi, Z. Meng, Z. An, Highly efficient room-temperature phosphorescence promoted via intramolecular-space heavy-atom effect, Adv. Opt. Mater. 11 (2023) 2201641, https://doi.org/10.1002/adom.202201641.
[19] Z. He, H. Gao, S. Zhang, S. Zheng, Y. Wang, Z. Zhao, D. Ding, B. Yang, Y. Zhang, W. Z. Yuan, Achieving persistent, efficient, and robust room-temperature phosphorescence from pure organics for versatile applications, Adv. Mater. 31 (2019) 1807222, https://doi.org/10.1002/adma.201807222.
[20] Z. Xiao, N. Li, W. Yang, Z. Huang, X. Cao, T. Huang, Z. Chen, C. Yang, Saccharin-derived multifunctional emitters featuring concurrently room temperature phosphorescence, thermally activated delayed fluorescence and aggregation-induced enhanced emission, Chem. Eng. J. 419 (2021) 129628, https://doi.org/10.1016/j.cej.2021.129628.
[21] X. Yang, S. Wang, K. Sun, H. Liu, M. Ma, S.T. Zhang, B. Yang, A Heavy-atom-free molecular motif based on symmetric bird-like structured tetraphenylenes with room-temperature phosphorescence (RTP) afterglow over 8 s, Angew. Chem. Int. Ed. 62 (2023) e202306475, https://doi.org/10.1002/anie.202306475.
[22] Y. Zhou, W. Qin, C. Du, H. Gao, F. Zhu, G. Liang, Long-lived room-temperature phosphorescence for visual and quantitative detection of oxygen, Angew. Chem. Int. Ed. 58 (2019) 12102–12106, https://doi.org/10.1002/anie.201906312.
[23] P. Long, Y. Feng, C. Cao, Y. Li, J. Han, S. Li, C. Peng, Z. Li, W. Feng, Self-protective room-temperature phosphorescence of fluorine and nitrogen codoped carbon dots, Adv. Funct. Mater. 28 (2018) 1800791, https://doi.org/10.1002/adfm.201800791.
[24] L. Deng, Z. Ma, J. Zhou, L. Chen, J. Wang, X. Qiao, D. Hu, D. Ma, J. Peng, Y. Ma, Regulating excited state of sulfone-locked triphenylamine heteroaromatics for high-efficiency ultralong room-temperature phosphorescence, Chem. Eng. J. 449 (2022) 137834, https://doi.org/10.1016/j.cej.2022.137834.
[25] K. Chen, Y. Jiang, Y. Zhu, Y. Lei, W. Dai, M. Liu, Z. Cai, H. Wu, X. Huang, Y. Dong, Host to regulate the T_1–S_1 and T_1–S_0 processes of guest excitons in doped systems to control the TADF and RTP emissions, J. Mater. Chem. C 10 (2022) 11607–11613, https://doi.org/10.1039/d2tc02167f.
[26] G. Li, Y. Li, X. Yang, J. Miao, Y. Cui, Y. Nie, S. Yang, W. Liu, G. Sun, N-to-S substitution induced fluorescence-to-phosphorescence dominant emission with excitation-dependent intersystem crossing, J. Mater. Chem. C 12 (2024) 2585–2592, https://doi.org/10.1039/d3tc00908d.
[27] H. Su, K. Hu, W. Huang, T. Wang, X. Zhang, B. Chen, H. Miao, X. Zhang, G. Zhang, Functional roles of polymers in room-temperature phosphorescent materials: modulation of intersystem crossing, air sensitivity and biological activity, Angew. Chem. Int. Ed. 62 (2023) e202218712, https://doi.org/10.1002/anie.202218712.
[28] Z. Wang, H. Qu, S. Xu, L. Yang, L. Bai, R. Liu, Promoting intersystem crossing by charge transfer state of dimers for persistent room temperature phosphorescence, Dyes Pigm. 222 (2024) 111870, https://doi.org/10.1016/j.dyepig.2023.111870.
[29] K. Narushima, Y. Kiyota, T. Mori, S. Hirata, M. Vacha, Suppressed triplet exciton diffusion due to small orbital overlap as a key design factor for ultralong-lived room-temperature phosphorescence in molecular crystals, Adv. Mater. 31 (2019) 1807268, https://doi.org/10.1002/adma.201807268.
[30] J. Guo, J. Liu, Y. Zhao, Y. Wang, L. Ma, J. Jiang, Time-dependent and clustering-induced phosphorescence, mechanochromism, structural-function relationships, and advanced information encryption based on isomeric effects and host-guest doping, Spectrochim. Acta. A. Mol. Biomol. Spectrosc. 317 (2024) 124449, https://doi.org/10.1016/j.saa.2024.124449.
[31] J. Guo, C. Yang, Y. Zhao, Long-lived organic room-temperature phosphorescence from amorphous polymer systems, Acc. Chem. Res. 55 (2022) 1160–1170, https://doi.org/10.1021/acs.accounts.2c00038.
[32] W. Ji, Y. Zhao, J. Guo, L. Ma, Y. Wang, Rapid construction and intrinsic mechanism of host-guest room temperature phosphorescence systems, Opt. Mater. 157 (2024) 116416, https://doi.org/10.1016/j.optmat.2024.116416.
[33] J. Jiang, J. Liu, C. Hu, Y. Wang, L. Ma, Construction and fine tuning of host-guest doping systems and the underlying mechanism of room temperature phosphorescence, Dyes Pigm. 222 (2024) 111931, https://doi.org/10.1016/j.dyepig.2023.111931.
[34] M. Li, X. Cai, Z. Chen, K. Liu, W. Qiu, W. Xie, L. Wang, S.J. Su, Boosting purely organic room-temperature phosphorescence performance through a host-guest strategy, Chem. Sci. 12 (2021) 13580–13587, https://doi.org/10.1039/d1sc03420k.
[35] Y. Xia, C. Zhu, F. Cao, Y. Shen, M. Ouyang, Y. Zhang, Host-guest doping in flexible organic crystals for room-temperature phosphorescence, Angew. Chem. Int. Ed. 62 (2023) e202217547, https://doi.org/10.1002/anie.202217547.
[36] B. Zhou, D. Yan, Stimuli-responsive organic phosphorescence through energy transfer, Sci. China Chem. 64 (2021) 509–510, https://doi.org/10.1007/s11426-021-9956-y.
[37] X. Dou, X. Wang, X. Xie, J. Zhang, Y. Li, B. Tang, Advances in polymer-based organic room-temperature phosphorescence materials, Adv. Funct. Mater. 34 (2024) 2314069, https://doi.org/10.1002/adfm.202314069.
[38] S. Liu, C. Li, L. Liao, Y. Huo, Z.-M. Su, F.-S. Liang, Y. Mu, Proton transfer induced persistent triplet charge transfer phosphorescence in molecule-doped polymer systems, Chem. Eng. J. 497 (2024) 154819, https://doi.org/10.1016/j.cej.2024.154819.
[39] Y. Zhao, L. Ma, Z. Huang, J. Zhang, I. Willner, X. Ma, H. Tian, Visible light activated organic room-temperature phosphorescence based on triplet-to-singlet förster-resonance energy transfer, Adv. Opt. Mater. 10 (2022) 2102701, https://doi.org/10.1002/adom.202102701.
[40] M. Gao, Y. Tian, X. Li, Y. Gong, M. Fang, J. Yang, Z. Li, The effect of molecular conformations and simulated "Self-Doping" in phenothiazine derivatives on room-temperature phosphorescence, Angew. Chem. Int. Ed. 62 (2023) e202214908, https://doi.org/10.1002/anie.202214908.
[41] Y. Wang, J. Yang, M. Fang, Y. Gong, J. Ren, L. Tu, B.Z. Tang, Z. Li, New phenothiazine derivatives that exhibit photoinduced room-temperature phosphorescence, Adv. Funct. Mater. 31 (2021) 2101719, https://doi.org/10.1002/adfm.202101719.
[42] Y. Hong, Y. Zhao, L. Ma, Y. Wang, Tuning triplet excitons and dynamic afterglow based on host-guest doping, Spectrochim. Acta. A. Mol. Biomol. Spectrosc. 324 (2025) 124955, https://doi.org/10.1016/j.saa.2024.124955.
[43] L. Shi, J. Liu, L. Ma, Y. Wang, The dual-band emission with long-lived thermally activated delayed fluorescence and room temperature phosphorescence by trace ingredient incorporation, Chem. Eng. J. 493 (2024) 152492, https://doi.org/10.1016/j.cej.2024.152492.
[44] H. Li, H. Ma, P. Zhang, Z. An, X. He, Modulating room-temperature phosphorescence of phenothiazine dioxide via external heavy atoms, Angew. Chem. Int. Ed. (2024) e202419366, https://doi.org/10.1002/anie.202419366.
[45] Y. Tian, J. Yang, Z. Liu, M. Gao, X. Li, W. Che, M. Fang, Z. Li, Multistage stimulus-responsive room temperature phosphorescence based on host-guest doping systems, Angew. Chem. Int. Ed. 60 (2021) 20259–20263, https://doi.org/10.1002/anie.202107639.
[46] X. Cai, Y. Sun, W. He, Y. Zheng, Y. Shi, Q. Cao, Multifunctional amino-boranes isomer room-temperature phosphorescent material: multi-substrate multicolor luminescence, multi-level anti-counterfeiting, light-controlled data erasing/writing, data Logic operation, and high anti-laundry detergent performance, Adv. Funct. Mater 34 (2024) 2407420, https://doi.org/10.1002/adfm.202407420.
[47] C. Chen, R. Huang, A.S. Batsanov, P. Pander, Y.T. Hsu, Z. Chi, F.B. Dias, M. R. Bryce, Intramolecular charge transfer controls switching between room temperature phosphorescence and thermally activated delayed fluorescence, Angew. Chem. Int. Ed. 57 (2018) 16407–16411, https://doi.org/10.1002/anie.201809945.
[48] J. Chen, J. Liu, L. Zeng, G. Dong, X. Guo, M. Sun, H. Liu, Y. Dong, C. Zhang, W. Li, Temperature-dependent reversible afterglow between green, orange, and red in dual-delay organic doped material, Adv. Opt. Mater. (2024) 2401660, https://doi.org/10.1002/adom.202401660.
[49] Q. Dang, L. Hu, J. Wang, Q. Zhang, M. Han, S. Luo, Y. Gong, C. Wang, Q. Li, Z. Li, Multiple luminescence responses towards mechanical stimulus and photo-induction: the key role of the stuck packing mode and tunable intermolecular interactions, Chem. Eur. J. 25 (2019) 7031–7037, https://doi.org/10.1002/chem.201901116.
[50] W. Qiao, M. Yao, J. Xu, H. Peng, J. Xia, X. Xie, Z. Li, Naphthyl substituted impurities induce efficient room temperature phosphorescence, Angew. Chem. Int. Ed. 62 (2023) e202315911, https://doi.org/10.1002/anie.202315911.
[51] Y. Wang, W. Dai, X. Qiu, Y. Lei, M. Liu, X. Wang, Y. Zhou, H. Wu, X. Huang, Host-guest doped room/high-temperature phosphorescence of diarylfuro[3,2-B]pyridine derivatives, Chem. Eng. J. 489 (2024) 150919, https://doi.org/10.1016/j.cej.2024.150919.
[52] P. Gao, K. Zhang, D. Ren, H. Liu, H. Zhang, H. Fu, L. Ma, D. Li, Host-guest chemistry of chiral mofs for multicolor circularly polarized luminescence including room temperature phosphorescence, Adv. Funct. Mater. 33 (2023) 2300105, https://doi.org/10.1002/adfm.202300105.
[53] F. Xiao, H. Gao, Y. Lei, W. Dai, M. Liu, X. Zheng, Z. Cai, X. Huang, H. Wu, D. Ding, Guest-host doped strategy for constructing ultralong-lifetime near-infrared organic phosphorescence materials for bioimaging, Nat. Commun. 13 (2022) 186, https://doi.org/10.1038/s41467-021-27914-0.
[54] X. Meng, Q. Hu, X. Wang, T. Ma, W. Liu, X. Zhu, C. Ye, Ultralong room-temperature phosphorescence from polycyclic aromatic hydrocarbons by accelerating intersystem crossing within a rigid polymer network, J. Mater. Chem. C 10 (2022) 17620–17627, https://doi.org/10.1039/d2tc02557d.
[55] C. Qian, X. Zhang, Z. Ma, X. Fu, Z. Li, H. Jin, M. Chen, H. Jiang, Z. Ma, Matrix-mediated color-tunable ultralong organic room temperature phosphorescence of 7 H -benzo[c]carbazole derivatives, CCS Chem. 6 (2024) 798–811, https://doi.org/10.31635/ccschem.023.202202561.
[56] S. Zhang, G. Liu, Z. Mao, S. Xue, Q. Sun, W. Yang, Organic dopant cyclization and significantly improved RTP properties, Chem. Sci. 15 (2024) 19886–19892, https://doi.org/10.1039/d4sc06213b.
[57] C. Wang, L. Qu, X. Chen, Q. Zhou, Y. Yang, Y. Zheng, X. Zheng, L. Gao, J. Hao, L. Zhu, B. Pi, C. Yang, Poly(arylene piperidine) quaternary ammonium salts promoting stable long-lived room-temperature phosphorescence in aqueous environment, Adv. Mater. 34 (2022), https://doi.org/10.1002/adma.202204415.